Transcriptional regulation profiling reveals PPARA-mediated fatty acid oxidation as a novel therapeutic target in phospholamban R14del cardiomyopathy

Magdalena Harakalova (M.Harakalova@umcutrecht.nl)
University Medical Center Utrecht https://orcid.org/0000-0002-7293-1029

Jiayi Pei
University Medical Center Utrecht

Renee Maas
University Medical Center Utrecht

Karen Gaar-Humphreys
University Medical Center Utrecht

Johannes Gho
University Medical Center Utrecht

Emilia Nagyova
University Medical Center Utrecht

Christian Snijders Blok
University Medical Center Utrecht

Iris van Adrichem
University Medical Center Utrecht

René van Es
University Medical Center Utrecht

Shahrzad Sepehrkhouy
University Medical Center Utrecht

Dries Feyen
Stanford University

Noortje van den Dungen
UMC Utrecht

Nico Lansu
University Medical Center Utrecht

Jorg Calis
University Medical Center Utrecht

Niels van der Kaaij
University Medical Center Utrecht https://orcid.org/0000-0002-3669-5209

Nicolaas de Jonge

University Medical Center Utrecht

Linda van Laake

University Medical Center Utrecht

Anneline ter Riele

UMCU

Manon Huibers

University Medical Center Utrecht

Roel de Weger

University Medical Center Utrecht

Marianne C. Verhaar

UMC Utrecht https://orcid.org/0000-0002-3276-6428

J. Peter van Tintelen

University Medical Center Utrecht, University of Utrecht https://orcid.org/0000-0003-3854-6749

Frederic Vaz

. Department of Clinical Chemistry, Amsterdam Gastroenterology & Metabolism, Laboratory Genetic Metabolic Diseases, Amsterdam UMC, University of Amsterdam https://orcid.org/0000-0002-9048-1041

Boudewijn Burgering

Uni

Alain van Mil

University Medical Center Utrecht

Jan Buikema

University Medical Center Utrecht

Aryan Vink

University Medical Center Utrecht https://orcid.org/0000-0002-9371-8788

Ioannis Karakikes

Stanford University

Mark Mercola

Stanford University https://orcid.org/0000-0002-1430-2013

Pieter AFM Doevendans

University Medical Center Utrecht https://orcid.org/0000-0002-6257-7169

Joost Sluijter

University Medical Center Utrecht

Frank van Steenbeek

University Medical Center Utrecht

Caroline Cheng

University Medical Center Utrecht

Michal Mokry

University Medical Center Utrecht https://orcid.org/0000-0002-5298-4852

Folkert Asselbergs

University Medical Center Utrecht https://orcid.org/0000-0002-1692-8669

Article

Keywords:

Posted Date: October 28th, 2022

DOI: https://doi.org/10.21203/rs.3.rs-1902254/v1

Abstract

Carriers of the R14del pathogenic variant in the phospholamban (*PLN*) gene develop severe cardiomyopathy with extracellular adipocyte infiltration and intracellular cardiomyocyte mitochondrial disturbances. However, the basis of this metabolic dysregulation tailoring potential treatment targets is unknown. Here, we present a combined approach of transcriptional regulation analysis in human primary tissue and validation in a unique long-term (160 days) matured human induced pluripotent stem cell-derived cardiomyocyte (hiPSC-CM) model. We demonstrate a dysregulated PPARA-mediated mitochondrial fatty acid oxidation (FAO) signalling in PLN-R14del hearts and hiPSC-CMs. PLN-R14del hiPSC-CMs also displayed a higher preference for glycolysis over FAO and presented limited flexibility in energy substrate switching leading to enhanced lipid droplet storage. By activating PPARA in PLN-R14del hiPSC-CMs using bezafibrate, we observed an improved mitochondrial structure and calcium handling function, further indicating the importance of FAO in the disease and the potential of PPARA agonists as a novel therapeutic strategy in cardiomyopathies.

Introduction

The R14del (c.40_42delAGA, p.Arg14del) pathogenic variant in the phospholamban (*PLN*) gene is associated with biventricular cardiomyopathy with a high risk of life-threatening ventricular arrhythmias, often presenting as dilated cardiomyopathy (DCM) or arrhythmogenic cardiomyopathy (ACM).[1,2] It explains a large proportion of Dutch DCM and ACM patients and has also been identified in many other countries.[3,4] PLN is a small phosphoprotein located in the cardiomyocyte sarcoplasmic reticulum and the nuclear membrane and is the major regulator of SERCA2a/ATP2A2 activity and calcium (Ca^{2+}) cycling.[1] We and others have shown that mechanisms within the nuclear, endoplasmic/sarcoplasmic reticulum and mitochondrial network are impaired in PLN-R14del cardiomyopathy.[5–7] Despite these efforts, no effective treatment is available for PLN-R14del variant carriers to prevent disease development.

Macroscopically, PLN-R14del hearts show biventricular subepicardial fibrofatty tissue replacement of the myocardium, which is characterised by extensive interstitial fibrosis, adipocyte infiltration, and islands of isolated cardiomyocytes between adipocytes.[8–10] This adipocyte infiltration and fibrosis create an anatomical barrier resulting in the reentry of the electrical impulse and thereby an increased risk of fatal arrhythmias.[11,12] A novel adult zebrafish *plna* R14del model also displays this adipocyte accumulation and mitochondrial damage in the diseased myocardium,[13] while the available murine models show mitochondrial impairment in the absence of adipocyte accumulation.[14,15] Mitochondrial dysfunction decreases ATP production, thereby opening the sensitive K^+ channels on the sarcolemma channels, which reduces cardiomyocyte excitability and impairs electrical conduction in the heart.[16] Besides altered electrical conduction, metabolic changes also affect cardiac ion channel gating, intracellular calcium handling, and fibrosis formation; all well-known aspects of PLN-R14del pathophysiology.[16] However, the majority of studies have focused on calcium regulation by PLN,[14,17] little effort has been put into elucidating the basis for the metabolic aberrations in human PLN-R14del cardiomyopathy.

The presence of myocardial fibrofatty infiltration is accompanied by intracellular cardiomyocyte lipid abnormalities in cardiomyopathies in adults, such as those due to variants in *PKP2* and *PNPLA2*.[18,19] Several forms of childhood cardiomyopathies caused by mutations in the mitochondrial fatty acid oxidation (FAO) pathway genes, such as *HADHA, HADHB, CPT2, and ACADVL*, also show intracellular cardiomyocyte lipid droplet storage and adipocyte infiltration in the myocardium and other organs.[20] A recent study has linked lipid droplet accumulation in PLN-R14del to the endoplasmic reticulum stress.[6] However, little is known about the transcriptional regulation of this process and what (metabolic) factors influence lipid droplet accumulation.

A limited number of lipid droplets, which store unutilized fatty acids (FAs) by mitochondria for energy production, are present in healthy cardiomyocytes. However, an increased lipid droplet deposition is associated with impaired FAO.[21] While FAs are the primary energy source in healthy adult cardiomyocytes, diseased cardiomyocytes switch from FAO to glycolysis for energy production, resembling the energy balance of the fetal heart.[22,23] Yet, this switch to fetus-like energy management is insufficient to meet adult energy consumption needs and it will disturb the capacity of FAO-based ATP synthesis, leading to further starvation of the heart and disease progression.[24] The impaired lipid metabolism could hereby contribute to the disease progression in PLN-R14del cardiomyocytes and warrant further investigation.

Here, we explored the role of transcriptional regulation on disturbed (lipid) metabolism in PLN-R14del cardiomyopathy. We showed that even after the removal of the dominant fibrofatty replacement in the subepicardial layer, the fingerprint of (lipid) metabolic dysregulation was still present in the remaining human myocardium. We further confirmed the disturbed (lipid) metabolism in human-induced pluripotent stem cell-derived cardiomyocytes (hiPSC-CMs) from PLN-R14del carriers. We also identified key transcription factors involved in the affected (lipid) metabolism, which can serve as promising targets for future therapeutic strategies. Furthermore, we examined the preference of energy sources and the metabolic flexibility in switching energy sources between PLN-R14del and wildtype hiPSC-CMs, including the effect of major energy substrate depletion. Finally, we employed two rescue methods, namely CRISPR/Cas9-based gene correction and an FAO-modulating compound (bezafibrate), to investigate the association of the PLN-R14del pathogenic variant with intracellular lipid accumulation, mitochondrial lipid metabolism and the Ca^{2+} handling properties. Collectively, our data on the negative effects of energy substrate dysregulation in PLN-R14del cardiomyopathy provide novel insights into the new therapeutic strategies and clinical practice (i.e. drug repurposing).

Methods

Full details are available in the Supplementary Material online. The study was approved by the local Biobank Research Ethics Committee and performed according to the Declaration of Helsinki.

Human cardiac tissues

Heart samples collected at autopsy or transplantation were obtained from a cohort of PLN-R14del variant positive patients (n = 6). Control hearts (n = 4) were obtained from donors that were not used for heart transplantation. To further elucidate the PLN-R14del-specific changes, hearts from patients with ischemic cardiomyopathy (n = 4) and non-ischemic cardiomyopathy based on pathogenic variants in genes encoding sarcomeric proteins (n = 6) were also included. The dominant fibrofatty replacement in the subepicardial layer, if present, was removed by a scalpel. The remaining compact myocardium was included in the study. An overview of cardiac tissues is presented in **Table S1A**.

Human-induced pluripotent stem cells-derived cardiomyocytes (hiPSC-CMs)

Wildtype control, PLN-R14del patient line, isogenic control (PLN-R14del was corrected by CRISPR/Cas9), homozygous line (knock-in in the PLN-R14del patient line), and carrier line (hiPSC-CMs derived from an asymptomatic PLN-R14del carrier) were generated under approved IRB and SCRO protocols and have been described previously. An overview of hiPSC-CMs is presented in **Table S1B**.

Multi-omics analyses

Since we and others have shown the importance of histone acetylation changes in heart diseases, including their regulation of gene expression, we performed ChIP-seq for H3K27ac on cardiac tissues as described previously. Differentially acetylated chromatin regions were identified between control and PLN-R14del hearts, followed by enrichment analysis of transcription factor binding motif, gene to peak annotation, and pathway enrichment analyses. Additionally, a set of PLN-R14del-specific histone acetylation changes were identified by further comparison to two non-PLN-R14del-related cardiomyopathy groups. RNA was isolated from cardiac tissues and hiPSC-CMs, followed by polyA selection, library preparation, and sequenced as described previously. Differentially expressed genes were identified using Deseq2 and gene set enrichment analyses were performed. For a detailed description, please refer to the online Supplementary Material.

Functional assays

First, the MTT (3-(4,5-dimethylthiazol-2-yl)-2,5-diphenyltetrazolium bromide) tetrazolium assay was used to examine the general metabolic activity of PLN-R14del and control hiPSC-CMs. Next, long-term cultured (77–159 days old) PLN-R14del and control hiPSC-CMs in three different culture media, including excessive access to FA or glucose, were included. Two main metabolic activities, namely FAO and glycolysis, were examined using a modified Seahorse XFe24 Extracellular Flux Analyzer. Etomoxir (ETO, a specific irreversible inhibitor of carnitine palmitoyltransferase 1) and 2-deoxy-D-glucose (2DG, a competitive glycolytic inhibitor) were applied to hiPSC-CMs separately to block FAO and glycolysis, respectively, and the dependence of hiPSC-CMs on these two pathways was determined by measuring the oxygen consumption rate (OCR) and extracellular acidification rate (ECAR). We also studied the the Ca^{2+} handling properties and the mitochondrial lipid metabolism by applying a FAO-modulating compound (bezafibrate) to PLN-R14del and control hiPSC-CMs for 24 hrs, followed by examining Ca^{2+} transient

parameters and activities of mitochondrial trifunctional protein. For a detailed description, please refer to the online Supplementary Material.

Multimodal microscopy

In frozen cardiac tissues from PLN-R14del and healthy individuals, Oil Red O staining was performed to detect lipid droplets. Electron microscopy was performed to further investigate intracellular lipid droplets present in these tissues. Candidate genes obtained from the multi-omics dataset, including ATP2A2, TNNI3, and FAO-related proteins (HADHA and PPARA), were examined and confirmed using immunofluorescence staining. Mitochondrial-related proteins (PPARA, ATP5F1A, and HSP60) and lipid droplets were examined and compared between short-term (25 days) and long-term cultured (160 days) hiPSC-CMs from PLN-R14del and healthy individuals using immunofluorescence staining. Nile red staining was also performed to compare lipid accumulation between PLN-R14del, wildtype control, isogenic control, homozygous, and carrier hiPSC-CMs.

Results

Identification of histone acetylation changes in PLN-R14del cardiac tissue

H3K27ac histone acetylation regulates gene transcription and contributes to phenotypic responses in heart diseases.[25] Therefore, we performed H3K27ac ChIP-seq to study histone acetylation changes in 6 PLN-R14del versus 4 control hearts (Fig. 1A and **Table S1A**). We identified 28,149 ± 9,538, and 25,721 ± 8,460 H3K27ac enriched regions within PLN-R14del and control hearts, respectively. We subsequently combined regions that were identified in at least two independent samples into a set of 23,356 regions to assess differentially acetylated regions between control and PLN-R14del groups. In total, 2,107 autosomal regions showed differential H3K27ac levels between PLN-R14del and control hearts (Fig. 1B and **Table S2A**). Compared to controls, regions with higher H3K27ac levels in PLN-R14del hearts are referred to as hyperacetylated regions (n = 1,149) and regions with lower H3K27ac levels in PLN-R14del hearts are referred to as hypoacetylated regions (n = 958, Fig. 1C and **Fig.S1**).

Genes annotated to differentially acetylated regions in PLN-R14del cardiac tissues are enriched in metabolic pathways

To identify genes potentially regulated by the differentially acetylated regions, we focused on regions in close vicinity to promoters and annotated genes 5,000 bases up- and downstream from the transcription start site of a gene as used previously (Fig. 1B**).**[25,26] Out of 968 hyperacetylated regions, 295 genes were identified in close vicinity to 251 hyperacetylated regions, and out of 1,149 hypoacetylated regions, 568 genes were identified in the close vicinity to 462 hypoacetylated regions (Fig. 1C, **Table S2B** and **2C**). To examine which biological processes and pathways are affected, we performed gene set enrichment analysis using genes annotated to differentially acetylated regions. We observed that hyperacetylation-

related genes were mostly involved in fibrosis, (cardiovascular) development, and chromatin assembly (**Table S2D** and **Fig.S2**), while hypoacetylation-related genes were related to metabolism (Fig. 1D and **Table S2E**).

The transcription factor binding motifs (TFBMs) overrepresented in hypoacetylated regions are enriched in metabolic pathways

To identify possible upstream acting transcription factors (TFs), which regulate genes involved in the pathogenesis of the disease, we studied the overrepresentation of TFBMs in differentially acetylated regions. By using the DNA sequences of all differentially acetylated regions in PLN-R14del versus control hearts (Fig. 1B), we detected enrichment in 202 TFBMs and annotated them to 200 TF-encoding genes (**Table S3A**). Consistently, several of the most enriched biological processes annotated to TFs pointed towards altered metabolism, such as adipogenesis and mitochondrial structure (**Table S3B** and **Fig.S3**). Notably, PPARA, a major regulator of cardiomyocyte lipid metabolism, particularly FAO, was also annotated from enriched motifs together with other interacting TFs (Fig. 1E). Therefore, we further investigated the localization of PPARA in cardiac tissues by immunofluorescence staining and observed a significant decrease in the nuclear PPARA signal of PLN-R14del cardiomyocytes versus the controls, whereas the PPARA signal in non-myocyte cells remained comparable between PLN-R14del and control hearts (Fig. 1F).

Hypoacetylated regions associated with metabolic pathways specific for PLN-R14del cardiomyopathy as compared to other cardiomyopathies

Besides non-failing control hearts, we also compared PLN-R14del hearts with other cardiomyopathies, including ischemic cardiomyopathy (n = 4) and non-ischemic dilated cardiomyopathy (sarcomeric group, n = 6, Fig. 1G). K-mean clustering analysis revealed four PLN-R14del-specific clusters when compared to other cardiomyopathy groups and the controls (Fig. 1H, **Fig.S4**, and **Table S4A**,). Genes located in the vicinity of these PLN-R14del-specific clusters were again highly enriched in metabolic signalling (**Table S4B and 4C**, and **Fig.S5**). Examples of metabolic genes, including *HADHA/ HADHB*, *SLC25A20*, *PDK2*, and *CPT1B*, which were annotated in PLN-R14del-specific hypoacetylated clusters were shown in Fig. 1I. Combined, we detected differentially acetylated regions that distinguish PLN-R14del from other types of cardiomyopathies and they annotated metabolic-related genes were profoundly affected.

Enriched metabolic pathways by differentially expressed genes in PLN-R14del hearts

Besides differentially acetylated regions, we obtained 1,668 up- and 1,873 downregulated genes in PLN-R14del versus control hearts using RNA-seq (Fig. 2A and Fig. 2B, **Table S5A**). In line with the well-established suppression of *SERCA2A/ATP2A2* at the protein level,[6] we showed its suppression at the

mRNA level for the first time. Additionally, metabolic genes, such as *HADHA* and *HAHDB*, which were annotated from PLN-R14del-specific hypoacetylated clusters, also showed significantly lower mRNA levels in PLN-R14del versus control hearts (Fig. 2C). We further demonstrated decreased HADHA and SERCA2A/ATP2A2 protein levels in PLN-R14del versus the control heart by immunofluorescence staining (Fig. 2D). Consistent with enriched biological processes and pathways by annotated genes from differentially acetylated regions, fibrosis, (cardiovascular) development, and chromatin assembly were enriched by upregulated genes (**Table S5B**) and metabolism (oxidative phosphorylation, ATP metabolic process, metabolic pathways, etc.) were enriched by downregulated genes **(**Fig. 2E and **Table S5C**).

Notably, among 200 TFs annotated from differentially acetylated regions, 39 TFs showed significantly altered mRNA levels in PLN-R14del versus control hearts, including 26 up- and 13 down-regulated TF-coding genes. Enriched protein-protein-interaction network by 39 TF-coding genes again suggests (negatively) affected metabolism (Fig. 2F). Thus, we identified a panel of upstream TFs and downstream targets in metabolic processes, which were disrupted in PLN-R14del cardiomyopathy.

Differentially expressed genes in PLN-R14del hiPSC-CMs suggest altered lipid metabolic pathways

Monolayers of hiPSC-CMs have been used to study the molecular mechanisms underlying several major cardiomyopathies, including ion-related, structural, and metabolic cardiomyopathies. However, the physiological immaturity of hiPSC-CMs severely limits their utility as a prediction model for adolescent genetic myopathies. To improve the cardiac immaturity limitation, we cultured hiPSC-CMs for 160 days in a maturation media designed to provide oxidative substrates adapted to the metabolic needs[27] (**Table S6)**. These long-term cultured hiPSC-CMs showed well-developed structural and mitochondrial organization as stained by the sarcomeric and mitochondrial marker **(Fig.S7A)**. Hereafter, we studied the transcriptome profiles in PLN-R14del and healthy control hiPSC-CMs (Fig. 3A and **Table S1B**).

First, we examined markers of cytoskeletal components (*ACTN1*, *TNNT2*, *MYH7*, and *MYL2*), ion channels (*KCNA5* and *KCNJ4*), and mitochondrial components (*ATP5F1A* and *HSP60*), and lipid metabolism (PPARA, ACAT1, FABP3, and Nile red staining). In general, we observed an increase in mRNA levels of most markers from short- and long-term (25 and 160 days, respectively) cultured PLN-R14del and healthy control hiPSC-CMs and confirmed these observations at the protein level by immunofluorescence staining (Fig. 3B and Fig. 3C). Therefore, we extended the culture time of hiPSC-CMs in the following experiments, which showed an overall improved maturation status but a more distinguishable metabolism-phenotype between PLN-R14del and control hiPSC-CMs.

Since our data obtained from PLN-R14del hearts indicated a disrupted lipid metabolism, we cultured control and PLN-R14del hiPSC-CMs to further elucidate the metabolic activities in three culture media containing different amounts of glucose and lipids, which are the two main metabolic substrates for cardiomyocytes (Fig. 3A). In total, we identified 952, 1,321, and 2,104 differentially expressed genes in PLN-R14del versus control hiPSC-CMs cultured in the maturation, the glucose-rich, and the lipid-rich medium, respectively (**Table S7A-C**). Notably, regardless of culture media, pathway enrichment analyses

using downregulated genes in PLN-R14del versus control hiPSC-CMs consistently pointed towards metabolic activities, such as oxidative phosphorylation/GO:0006119 (Fig. 3D, **Fig.S8A-C**, and **Table S7D-F**). However, it is important to note that the metabolic genes involved in the enriched biological processes (i.e., oxidative phosphorylation), which were shared among three conditions, were not the same (**Fig.S8D-F**). Similarly, regardless of culture media, pathway enrichment analyses using upregulated genes in PLN-R14del versus control hiPSC-CMs consistently pointed towards fibrosis and (cardiovascular) development, which were in line with the results obtained from the *ex vivo* human cardiac tissues (**Table S7D-F**).

Disturbed fatty acid oxidation (FAO) and metabolic flexibility in PLN-R14del hiPSC-CMs

Besides the downregulated transcriptional regulation of lipid metabolism in PLN-R14del cardiomyopathy, a significantly lower cellular metabolic activity/viability was also observed in PLN-R14del versus control hiPSC-CMs (Fig. 4A). This suppression remained when excessive glucose or FAs were given to the cells (**Fig.S7B-C**). To further elucidate whether the obtained transcriptomic data could predict affected metabolism in PLN-R14del cardiomyopathy, we compared the FAO metabolism, a key metabolic program in cardiomyocytes (Fig. 4B), by evaluating mitochondrial respiration via ETO-inhibited FAO and 2-DG-inhibited glycolysis using the Seahorse analysis (Fig. 4C).

In the maturation medium, which contains both glucose and FAs, we observed a comparable oxygen consumption rate (OCR) between PLN-R14del and control hiPSC-CMs at the baseline level and after ETO-inhibited FAO (Fig. 4E), suggesting a similar FAO-dependence of both groups. However, after blocking glycolysis by 2-DG, we observed an increased OCR in control hiPSC-CMs, whereas the OCR of PLN-R14del hiPSC-CMs continued to decline significantly, suggesting control hiPSC-CMs are less dependent on glycolysis and have more metabolic adaptive characteristics than PLN-R14del hiPSC-CMs.

Similarly, in the glucose-rich medium, OCR was comparable between PLN-R14del and control hiPSC-CMs at the baseline level (Fig. 4F). After blocking glycolysis, a significantly higher OCR was observed in control versus PLN-R14del hiPSC-CMs, once again suggesting better metabolic flexibility and substrate utilisation in control hiPSC-CMs.

Notably, in the lipid-rich medium, the basal OCR was significantly lower in PLN-R14del versus control hiPSC-CMs (Fig. 4G), implying an impaired FAO in the PLN-R14del hiPSC-CMs at the beginning. Although OCRs of both PLN-R14del and control hiPSC-CMs decreased after FAO- and glycolysis-blockages, OCRs remained significantly lower in PLN-R14del hiPSC-CMs than in the controls. These findings suggest that despite the presence of excess lipids in the medium, PLN-R14del hiPSC-CMs are less capable of utilizing their FAO metabolism to produce the required energy, therefore being more glycolysis-dependent.

Higher glucose dependency in PLN-R14del hiPSC-CMs

Glucose metabolism, another major metabolic program in cardiomyocytes (Fig. 4B), was also studied. We measured the extracellular acidification rate (ECAR) to study the activity of the glycolytic pathway in PLN-

R14del and wild-type hiPSC-CMs by manipulating the FAO and glucose metabolism using ETO and 2-DG respectively (Fig. 4D).

In the maturation medium, basal ECAR levels were comparable between both groups, but it became significantly lower in PLN-R14del versus control hiPSC-CMs after FAO- and glycolysis-blockages (Fig. 4H), indicating a higher glycolysis dependency of PLN-R14del hiPSC-CMs. A significantly higher glycolytic reserve was also observed in PLN-R14del hiPSC-CMs than in the controls.

In the glucose-rich medium, ECAR levels remained comparable between both groups at the basal level, after blocking FAO, and after blocking glycolysis (Fig. 4I). However, the decline of ECAR after glycolysis-blockage was more profound in PLN-R14del versus control hiPSC-CMs, suggesting a higher glycolysis-dependence and a higher glycolytic reserve of PLN-R14del hiPSC-CMs.

In the lipid-rich medium, basal ECAR levels were comparable between both groups (Fig. 4J). Interestingly, a higher ECAR was shown in PLN-R14del versus control hiPSC-CMs after FAO-blockage, which decreased profoundly after glycolysis-blockage, again, confirming the higher glycolysis-dependency in PLN-R14del hiPSC-CMs. These results imply our *in vitro* maturation-induced PLN-R14del hiPSC-CM mimics the heart failure-related metabolic alterations consisting of the energy production reduction by mitochondria through oxidative phosphorylation and an increase in (anaerobic) glycolysis.

Intracellular lipid droplet accumulation is a key feature of PLN-R14del cardiomyopathy

Data acquired from the cardiac tissues and/or hiPSC-CMs at DNA, RNA, protein, and functional levels consistently pointed towards altered metabolism in PLN-R14del versus control groups, particularly FAO. Since lipid accumulation is known as the hallmark of impaired FAO, we examined the lipid accumulation in cardiac tissues and hiPSC-CMs.

First, we performed a digital quantification in heart slices assessing the percentage of adipose tissue, which showed an increased adipocyte deposition in PLN-R14del versus control hearts (**Fig.S8**). Next, we used Nile red to localise intracellular lipid droplets in snap-frozen and paraffin-embedded tissues and observed a more frequent perinuclear accumulation of lipid droplets in PLN-R14del cardiac tissue than in the control (Fig. 5A**)**. Transmission electron microscopy revealed a significantly lower mitochondrial length (aspect ratio) and a significantly higher accumulation of intracellular lipid droplets in PLN-R14del versus control hearts (Fig. 5B and Fig. 5C), suggesting impaired mitochondrial FAO. In line with the hearts, highly accumulated intracellular lipid droplets were observed in PLN-R14del versus control hiPSC-CMs, regardless of different culturing media (Fig. 5D). Combined, these findings suggested intracellular lipid droplet accumulation is a key feature in PLN-R14del cardiomyopathy.

CRISPR/Cas9-based correction of PLN-R14del attenuated intracellular lipid accumulation

We used CRISPR/Cas9-based gene editing to correct PLN-R14del mutation[28] and observed a significant reduction of intracellular lipid droplets in R14del-corrected hiPSC-CMs (isogenic control, Fig. 6A). Interestingly, hiPSC-CMs derived from an asymptomatic PLN-R14del carrier and the homozygous hiPSC-CMs showed a comparable amount of the lipid droplets as in PLN-R14del hiPSC-CMs. These findings suggested a tight relationship between PLN-R14del mutation and impaired lipid metabolism, thereby leading to intracellular lipid droplet accumulation.

PPARA-targeted drug increased Ca^{2+} handling and mitochondrial trifunctional protein levels in PLN-R14del hiPSC-CMs

We also applied a PPARA agonist (bezafibrate) to further investigate PPARA-mediated FAO in PLN-R14del cardiomyocytes. First, we measured the Ca^{2+} transient in control and PLN-R14del hiPSC-CMs with and without bezafibrate treatment. We observed significantly increased rise and decay time in treated versus untreated PLN-R14del hiPSC-CMs (Fig. 6B), whereas the treatment did not affect Ca^{2+} handling in control hiPSC-CMs. Next, we examined HADHA and HADHB levels, encoding the mitochondrial trifunctional protein involved in the FAO pathway, which showed suppressed histone acetylation and transcriptional levels in PLN-R14del versus control hearts (Fig. 1I and Fig. 2C). We confirmed the suppression of HADHA and HADHB in long-term cultured untreated PLN-R14del cardiomyocytes and further showed elevated HADHA and HADHB levels in bezafibrate-treated PLN-R14del cardiomyocytes (Fig. 6C). Whereas, the treatment did not alter HADHA and HADHB levels in control hiPSC-CMs. Combined, these findings suggested disturbed HADHA/HADHB-involved FAO in PLN-R14del hiPSC-CMs, the potential association between PPARA-mediated FAO and Ca^{2+} handling, and the role of PPARA as a promising therapeutic target in PLN-R14del cardiomyopathy.

Discussion

In this study, we provide new information on changes in chromatin activity and global transcriptional regulation in human myocardium obtained from patients with PLN-R14del cardiomyopathy compared to other types of cardiomyopathy and healthy controls. Multi-omics integration points to the inhibited mitochondrial function and (lipid) metabolism in PLN-R14del hearts based on the changed histone acetylation levels of annotated gene promoters, predicted TFBMs and altered gene expression. These datasets will serve as the basis for upcoming biomarker and novel therapeutic strategies.

We particularly focused on the inhibited PPARA-mediated FAO in PLN-R14del hearts. PPARA is a key TF that regulates cardiac lipid metabolism to enhance FAO.[29] It is predominantly located within the nucleus,[30] however, external signals and pathways regulate the transport of PPARA from the nucleus to other subcellular compartments and mediate the biological functions of PPARA.[31] We obtained the enriched TFBM of PPARA in differentially acetylated promoters between PLN-R14del and controls. Although the histone acetylation of *PPARA* promoter and mRNA level of *PPARA* remained comparable

between PLN-R14del and control hearts, we showed a significant decline of PPARA signal inside cardiomyocyte nuclei in PLN-R14del hearts. Taken together, the loss of nuclear PPARA in PLN-R14del cardiomyocytes suggested suppressed PPARA-mediated biological processes that take place inside nuclei, including substrate inflexibility promoting FFA uptake and lipid accumulation, and ensuing cardiovascular complications.

The promoters of PPARA-regulated downstream targets in lipid metabolism, such as *HADHA*, *HADHB*, *MLYCD*, and *PNPLA2*,[32,33,34] showed suppressed acetylation levels in PLN-R14del hearts. Furthermore, by comparing PLN-R14del hearts with non-PLN-R14del-related cardiomyopathies, we identified PLN-R14del-specific regions and many annotated genes in these regions also involved in lipid metabolism (e.g. *AGPAT2*, *HADHA*, *HADHB*, *MLYCD*, *PLPP1*, and *PTGDS*). Additionally, several of these metabolic genes also showed decreased mRNA levels in PLN-R14del versus control hearts, including *HADHA* and *HADHB*. In line with these omics-based data, we also observed accumulated lipid droplets and abnormal mitochondrial morphology in PLN-R14del hearts. Combined, the impaired PPARA-regulated FAO could play a critical role in PLN-R14del cardiomyopathy.

A recent study also showed that 18–33 days old PLN-R14del engineered heart tissues had impaired energy metabolism reflected at the protein level, including suppressed FAs metabolism and accumulation of lipid droplets.[6] Here, we further explored and identified affected genes in the metabolic regulation in long-term cultured PLN-R14del and control hiPSC-CMs (> 110 days). We demonstrated for the first time that PLN-R14del hiPSC-CMs displayed a lower FAO profile than the controls at both mRNA and functional levels, and this suppression pattern remained consistent even though PLN-R14del hiPCS-CMs were given excessive amounts of FAs or glucose, indicating the profoundly impaired lipid metabolism. FAO changes serve as an indicator of an early adapted or maladapted metabolic response.[35] Normally, the majority of the energy demand of the heart comes from mitochondrial FAO, especially free circulating FAs.[36] In contrast, diseased cardiomyocytes suffer from a decreased FAO and an increased intracellular lipid accumulation resulting in lipotoxicity and cell death.[37,38] We also showed lipid accumulation and a decreased cell viability of PLN-R14del hiPSC-CMs, further suggesting the importance of impaired FAO as a key pathological mechanism underling PLN-R14del cardiomyopathy.

Notably, we observed enhanced Ca^{2+} handling properties and elevated mitochondrial trifunctional protein levels (HADHA and HADHB) in PLN-R14del hiPSC-CMs after bezafibrate treatment, a PPARA-targeting agonist. Several FDA/EMA-approved PPARA agonists, including bezafibrate, have shown protective effects on cardiomyopathies by restoring the FA metabolism.[39,40] However, to the best of our knowledge, we showed for the first time, the potential of bezafibrate in re-activating mitochondrial FAO and improving Ca^{2+} transients, which provides a novel strategic path for developing precision medicine for PLN-R14del patients, such as targeting FAO upstream regulators (i.e. PPARA).

Besides FAO suppression, the activation of glycolysis-related genes was shown in murine cardiomyocytes carrying another *PLN* pathogenic variant (p.Arg9Cys).[41] We also showed PLN-R14del hiPSC-CMs

exhibited a preference for glucose utilisation. Increased glucose utilisation, which further inhibits FAO by malonyl coenzyme A-mediated inhibition, has been shown in cardiomyocytes from hypertrophic cardiomyopathies and failing hearts.[33,42] The switch from FAs to glucose utilisation can be due to its faster uptake in the cells and the lower oxygen consumption.[43] Like lipotoxicity, increased glucose levels can have deleterious effects on cardiomyocytes by introducing oxidative stress-related cell death and decreasing contractile force.[44,45] Thus, the glucose-dependent energy metabolism is associated with the progression of cardiac dysfunction and could be an early pathological process in PLN-R14del hearts.[42]

Last but not least, we also observed reduced metabolic flexibility in PLN-R14del hiPSC-CMs. Healthy cardiomyocytes have the flexibility of switching substrates for energy production under different conditions.[42] This metabolic flexibility is a critical factor for maintaining normal cardiac function and preventing the progression of diseased hearts.[46] Impaired metabolic flexibility has also been observed in mouse cardiomyocytes with the depletion of *Ryr2*, which show reduced mRNA levels of key regulators in the FA metabolism (e.g. *Ppargc1a*, *Pparα*, *Pparγ*, and *Klf15*) as well as the glucose metabolism (e.g. *Glut4* and *Pck1*).[47] Therefore, restoring balanced metabolic activity is beneficial for PLN-R14del cardiomyopathy.

It is important to note that histone acetylation and transcriptome changes in PLN-R14del versus control hearts are derived from both cardiomyocytes and non-myocyte cell types, such as endothelial cells and fibroblasts that are abundant in the heart.[48] Non-myocyte cell types in the heart also contribute to the disease progression.[49] Therefore, the responsible cell type(s) or mechanisms for the adipocyte infiltration by either the activation of the already existing pool of adipocytes or transdifferentiation of (cardiac) cells into adipocytes remain unclear. However, we have previously shown that the majority of the bulk data came from cardiomyocytes when compared to 11 non-myocyte cell types in both inherited and acquired heart disease.[25,26] The impaired mitochondrial FAO indicated by the bulk data was validated in PLN-R14del hiPSC-CMs at transcriptional and functional levels, highlighting the possibility of FAO abnormalities as early pathological signs in PLN-R14del cardiomyocytes. Nevertheless, future studies should also focus on investigating interactions between cardiomyocytes and non-myocyte cells during the cardiac energy rearrangement as well as the impact of lipid disturbances in PLN-R14del cardiomyopathy.

In conclusion, we revealed valuable information on the histone acetylation activities and the transcriptome regulation in PLN-R14del hearts and PLN-R14del hiPSC-CMs when compared with controls. Integrating this data, we demonstrated a disturbed energy metabolism in PLN-R14del and identified upstream TFs regulating impaired FAO. CRISPR-Cas9-based therapy to correct PLN-R14del and bezafibrate treatment to re-active mitochondrial FAO further illustrated the tight relationships between the mutation, imapired FAO, lipid accumulation, and Ca^{2+} handling and sheld light to future therapeutic strategies for PLN-R14del patients.

Declarations

ACKNOWLEDGMENTS

We are very thankful to the patients and their families for providing valuable cardiac tissue for research purposes. We further thank Marc P. Buijsrogge (in memoriam) for collecting cardiac tissues and Joyce van Kuik, Erica Sierra-de Koning and Petra van der Kraak for technical assistance with tissue processing. We thank Utrecht Sequencing Facility for providing sequencing service and data. Utrecht Sequencing Facility is subsidised by the University Medical Centre Utrecht, Hubrecht Institute, Utrecht University and The Netherlands X-omics Initiative (NWO project 184.034.019). We thank Prof. Joseph C. Wu from Stanford University for providing lines SCVI-111 and SCVI-273. Both first shared authors contributed equally and have the right to put their names forward for CV purposes.

SOURCES OF FUNDING

This work was supported by the Dutch PLN patient organisation Foundation PLN (JYP, RGCM, MH, JMIHG, FWA), Leducq grant (CURE-PLaN no. 18CVD01 to JYP, RGCM, JC, DF, IK, MM, PAD, JPvT,, MH, FWA), the NWO VENI grant (no. 016.176.136 to MH), ZonMW Open Competition grant (CONTRACT no. 09120012010018 to KGH, FWA, MH), National Institute of Health grants R01 LM010098 (MH, FWA) and R01HL152055, P01HL141084 (MM), Dutch Cardiovascular Alliance (DCVA) grant (DOUBLE-DOSE no. 2020B005 to MH, FvS, FWA, JPvT), ERA-CVD grant (SCALE no. 2019T109 to JYP, FvS, MH), Netherlands Foundation for Cardiovascular Excellence (CC), two NWO VIDI grants (no. 91714302 to CC and no. 016096359 to MCV), the ErasmusMC fellowship grant (CC), the RM fellowship grant of the UMC Utrecht (CC), and UCL Hospitals NIHR Biomedical Research Centre grant BRC86A (FWA), Horizon2020 ERC-2016-COG EVICARE (725229), Horizon 2020 BRAV3 (SC1-BHC-07-2019), NWO-TTP program (Harvey 2021/TTW/01038252), and ZonMW-PSIDER (ZonMw file No: 40-46800-98-018) to JS.

DISCLOSURES

None

References

1. Haghighi K, Kolokathis F, Gramolini AO, Waggoner JR, Pater L, Lynch RA, Fan G-C, Tsiapras D, Parekh RR, Dorn GW, II, MacLennan DH, Kremastinos DT, Kranias EG. A mutation in the human phospholamban gene, deleting arginine 14, results in lethal, hereditary cardiomyopathy. Proc Natl Acad Sci U S A. 2006;103:1388.
2. van Rijsingen IAW, van der Zwaag PA, Groeneweg JA, Nannenberg EA, Jongbloed JDH, Zwinderman AH, Pinto YM, Dit Deprez RHL, Post JG, Tan HL, de Boer RA, Hauer RNW, Christiaans I, van den Berg MP, van Tintelen JP, Wilde AAM. Outcome in phospholamban R14del carriers: results of a large multicentre cohort study. Circ Cardiovasc Genet. 2014;7:455–465.
3. Hof IE, van der Heijden JF, Kranias EG, Sanoudou D, de Boer RA, van Tintelen JP, van der Zwaag PA, Doevendans PA. Prevalence and cardiac phenotype of patients with a phospholamban mutation.

Neth Heart J. 2019;27:64–69.

4. Doevendans PA, Glijnis PC, Kranias EG. Leducq Transatlantic Network of Excellence to Cure Phospholamban-Induced Cardiomyopathy (CURE-PLaN). Circ Res. 2019;125:720–724.
5. Karakikes I, Stillitano F, Nonnenmacher M, Tzimas C, Sanoudou D, Termglinchan V, Kong C-W, Rushing S, Hansen J, Ceholski D, Kolokathis F, Kremastinos D, Katoulis A, Ren L, Cohen N, Gho JMIH, Tsiapras D, Vink A, Wu JC, Asselbergs FW, Li RA, Hulot J-S, Kranias EG, Hajjar RJ. Correction of human phospholamban R14del mutation associated with cardiomyopathy using targeted nucleases and combination therapy. Nat Commun. 2015;6:6955.
6. Cuello F, Knaust AE, Saleem U, Loos M, Raabe J, Mosqueira D, Laufer S, Schweizer M, van der Kraak P, Flenner F, Ulmer BM, Braren I, Yin X, Theofilatos K, Ruiz-Orera J, Patone G, Klampe B, Schulze T, Piasecki A, Pinto Y, Vink A, Hübner N, Harding S, Mayr M, Denning C, Eschenhagen T, Hansen A. Impairment of the ER/mitochondria compartment in human cardiomyocytes with PLN p.Arg14del mutation. EMBO Mol Med. 2021;13:e13074.
7. Te Rijdt WP, van Tintelen JP, Vink A, van der Wal AC, de Boer RA, van den Berg MP, Suurmeijer AJH. Phospholamban p.Arg14del cardiomyopathy is characterized by phospholamban aggregates, aggresomes, and autophagic degradation. Histopathology. 2016;69:542–550.
8. Gho JMIH, van Es R, Stathonikos N, Harakalova M, te Rijdt WP, Suurmeijer AJH, van der Heijden JF, de Jonge N, Chamuleau SAJ, de Weger RA, Asselbergs FW, Vink A. High resolution systematic digital histological quantification of cardiac fibrosis and adipose tissue in phospholamban p.Arg14del mutation associated cardiomyopathy. PLoS One. 2014;9:e94820.
9. Te Rijdt WP, Asimaki A, Jongbloed JDH, Hoorntje ET, Lazzarini E, van der Zwaag PA, de Boer RA, van Tintelen JP, Saffitz JE, van den Berg MP, Suurmeijer AJH. Distinct molecular signature of phospholamban p.Arg14del arrhythmogenic cardiomyopathy. Cardiovasc Pathol. 2019;40:2–6.
10. Sepehrkhouy S, Gho JMIH, van Es R, Harakalova M, de Jonge N, Dooijes D, van der Smagt JJ, Buijsrogge MP, Hauer RNW, Goldschmeding R, de Weger RA, Asselbergs FW, Vink A. Distinct fibrosis pattern in desmosomal and phospholamban mutation carriers in hereditary cardiomyopathies. Heart Rhythm. 2017;14:1024–1032.
11. Justus M. B. Anumonwo TH. Fatty Infiltration of the Myocardium and Arrhythmogenesis: Potential Cellular and Molecular Mechanisms. *Front Physiol* [Internet]. 2018 [cited 2020 May 18];9. Available from: https://www.ncbi.nlm.nih.gov/pmc/articles/PMC5786512/
12. Te Rijdt WP, Ten Sande JN, Gorter TM, van der Zwaag PA, van Rijsingen IA, Boekholdt SM, van Tintelen JP, van Haelst PL, Planken RN, de Boer RA, Suurmeijer AJH, van Veldhuisen DJ, Wilde AAM, Willems TP, van Dessel PFHM, van den Berg MP. Myocardial fibrosis as an early feature in phospholamban p.Arg14del mutation carriers: phenotypic insights from cardiovascular magnetic resonance imaging. Eur Heart J Cardiovasc Imaging. 2019;20:92–100.
13. Kamel SM, van Opbergen CJM, Koopman CD, Verkerk AO, Boukens BJD, de Jonge B, Onderwater YL, van Alebeek E, Chocron S, Polidoro Pontalti C, Weuring WJ, Vos MA, de Boer TP, van Veen TAB, Bakkers J. Istaroxime treatment ameliorates calcium dysregulation in a zebrafish model of

phospholamban R14del cardiomyopathy. *Nat Commun* [Internet]. 2021 [cited 2022 Jan 27];12. Available from: https://www.ncbi.nlm.nih.gov/pmc/articles/PMC8660846/

14. Eijgenraam TR, Boukens BJ, Boogerd CJ, Marloes Schouten E, van de Kolk CWA, Stege NM, te Rijdt WP, Hoorntje ET, van der Zwaag PA, van Rooij E, van Tintelen JP, van den Berg MP, van der Meer P, van der Velden J, Silljé HHW, de Boer RA. The phospholamban p.(Arg14del) pathogenic variant leads to cardiomyopathy with heart failure and is unreponsive to standard heart failure therapy. Sci Rep. 2020;10:1–13.
15. Raad N, Bittihn P, Cacheux M, Jeong D, Ilkan Z, Ceholski D, Kohlbrenner E, Zhang L, Cai CL, Kranias EG, Hajjar RJ, Stillitano F, Akar FG. Arrhythmia Mechanism and Dynamics in a Humanized Mouse Model of Inherited Cardiomyopathy Caused by Phospholamban R14del Mutation. *Circulation* [Internet]. 2021 [cited 2022 Jan 27];144. Available from: https://pubmed.ncbi.nlm.nih.gov/34024116/
16. van Opbergen CJM, den Braven L, Delmar M, van Veen TAB. Mitochondrial Dysfunction as Substrate for Arrhythmogenic Cardiomyopathy: A Search for New Disease Mechanisms. *Front Physiol* [Internet]. 2019 [cited 2022 Apr 14];0. Available from: http://dx.doi.org/10.3389/fphys.2019.01496
17. Haghighi K, Gardner G, Vafiadaki E, Kumar M, Green LC, Ma J, Crocker JS, Koch S, Arvanitis DA, Bidwell P, Rubinstein J, van de Leur R, Doevendans PA, Akar FG, Tranter M, Wang H-S, Sadayappan S, DeMazumder D, Sanoudou D, Hajjar RJ, Stillitano F, Kranias EG. Impaired Right Ventricular Calcium Cycling Is an Early Risk Factor in R14del-Phospholamban Arrhythmias. *Journal of Personalized Medicine* [Internet]. 2021 [cited 2022 Jul 25];11. Available from: https://www.ncbi.nlm.nih.gov/pmc/articles/PMC8226909/
18. Shah K, Wei C-Y, Kim C-S, Wong J, Wen J-Y, Tirasawasdichai T, Wang C, -S. Vincent Chen H. Modeling Arrhythmogenic Right Ventricular Dysplasia/Cardiomyopathy with Patient-Specific iPSCs. In: Human iPS Cells in Disease Modelling. Springer, Tokyo; 2016. p. 27–43.
19. Haemmerle G, Moustafa T, Woelkart G, Büttner S, Schmidt A, van de Weijer T, Hesselink M, Jaeger D, Kienesberger PC, Zierler K, Schreiber R, Eichmann T, Kolb D, Kotzbeck P, Schweiger M, Kumari M, Eder S, Schoiswohl G, Wongsiriroj N, Pollak NM, Radner FPW, Preiss-Landl K, Kolbe T, Rülicke T, Pieske B, Trauner M, Lass A, Zimmermann R, Hoefler G, Cinti S, Kershaw EE, Schrauwen P, Madeo F, Mayer B, Zechner R. ATGL-mediated fat catabolism regulates cardiac mitochondrial function via PPAR-α and PGC-1. Nat Med. 17:1076.
20. Lawrence Merritt J, II, Norris M, Kanungo S. Fatty acid oxidation disorders. *Annals of Translational Medicine* [Internet]. 2018 [cited 2021 Mar 12];6. Available from: https://www.ncbi.nlm.nih.gov/pmc/articles/PMC6331364/
21. Christian Schulze P, Drosatos K, Goldberg IJ. Lipid Use and Misuse by the Heart. Circ Res. 2016;118:1736.
22. Osorio JC, Stanley WC, Linke A, Castellari M, Diep QN, Panchal AR, Hintze TH, Lopaschuk GD, Recchia FA. Impaired Myocardial Fatty Acid Oxidation and Reduced Protein Expression of Retinoid X Receptor-α in Pacing-Induced Heart Failure [Internet]. Circulation. 2002;106:606–612. Available from: http://dx.doi.org/10.1161/01.cir.0000023531.22727.c1

23. Carvajal K, Moreno-Sánchez R. Heart Metabolic Disturbances in Cardiovascular Diseases [Internet]. Archives of Medical Research. 2003;34:89–99. Available from: http://dx.doi.org/10.1016/s0188-4409(03)00004-3
24. Dávila-Román VG, Vedala G, Herrero P, de las Fuentes L, Rogers JG, Kelly DP, Gropler RJ. Altered myocardial fatty acid and glucose metabolism in idiopathic dilated cardiomyopathy. J Am Coll Cardiol. 2002;40:271–277.
25. Pei J, Harakalova M, Treibel TA, Lumbers RT, Boukens BJ, Efimov IR, van Dinter JT, González A, López B, El Azzouzi H, van den Dungen N, van Dijk CGM, Krebber MM, den Ruijter HM, Pasterkamp G, Duncker DJ, Nieuwenhuis EES, de Weger R, Huibers MM, Vink A, Moore JH, Moon JC, Verhaar MC, Kararigas G, Mokry M, Asselbergs FW, Cheng C. H3K27ac acetylome signatures reveal the epigenomic reorganization in remodeled non-failing human hearts. Clin Epigenetics. 2020;12:1–18.
26. Pei J, Schuldt M, Nagyova E, Gu Z, el Bouhaddani S, Yiangou L, Jansen M, Calis JJA, Dorsch LM, Blok CS, van den Dungen NAM, Lansu N, Boukens BJ, Efimov IR, Michels M, Verhaar MC, de Weger R, Vink A, van Steenbeek FG, Baas AF, Davis RP, Uh HW, Kuster DWD, Cheng C, Mokry M, van der Velden J, Asselbergs FW, Harakalova M. Multi-omics integration identifies key upstream regulators of pathomechanisms in hypertrophic cardiomyopathy due to truncating MYBPC3 mutations. Clin Epigenetics. 2021;13:1–20.
27. Feyen DAM, McKeithan WL, Bruyneel AAN, Spiering S, Hörmann L, Ulmer B, Zhang H, Briganti F, Schweizer M, Hegyi B, Liao Z, Pölönen RP, Ginsburg KS, Lam CK, Serrano R, Wahlquist C, Kreymerman A, Vu M, Amatya PL, Behrens CS, Ranjbarvaziri S, Maas RGC, Greenhaw M, Bernstein D, Wu JC, Bers DM, Eschenhagen T, Metallo CM, Mercola M. Metabolic Maturation Media Improve Physiological Function of Human iPSC-Derived Cardiomyocytes. *Cell Rep* [Internet]. 2020 [cited 2022 Mar 22];32. Available from: https://pubmed.ncbi.nlm.nih.gov/32697997/
28. Feyen DAM, Perea-Gil I, Maas RGC, Harakalova M, Gavidia AA, Arthur AJ, Wu TH, Vink A, Pei J, Vadgama N, Suurmeijer AJ, Te Rijdt WP, Vu M, Amatya PL, Prado M, Zhang Y, Dunkenberger L, Sluijter JPG, Sallam K, Asselbergs FW, Mercola M, Karakikes I. Unfolded Protein Response as a Compensatory Mechanism and Potential Therapeutic Target in PLN R14del Cardiomyopathy. *Circulation* [Internet]. 2021 [cited 2022 Jan 24];144. Available from: https://pubmed.ncbi.nlm.nih.gov/33928785/
29. Finck BN. The PPAR regulatory system in cardiac physiology and disease. Cardiovasc Res. 2007;73:269–277.
30. Grygiel-Górniak B. Peroxisome proliferator-activated receptors and their ligands: nutritional and clinical implications - a review. Nutr J. 2014;13:1–10.
31. Umemoto T, Fujiki Y. Ligand-dependent nucleo-cytoplasmic shuttling of peroxisome proliferator-activated receptors, PPARα and PPARγ. *Genes Cells* [Internet]. 2012 [cited 2022 Mar 2];17. Available from: https://pubmed.ncbi.nlm.nih.gov/22646292/
32. Schuier AM, Wood PA. Mouse Models for Disorders of Mitochondrial Fatty Acid β-Oxidation. ILAR J. 2002;43:57–65.

33. van Weeghel M, Abdurrachim D, Nederlof R, Argmann CA, Houtkooper RH, Hagen J, Nabben M, Denis S, Ciapaite J, Kolwicz SC, Lopaschuk GD, Auwerx J, Nicolay K, Des Rosiers C, Wanders RJ, Zuurbier CJ, Prompers JJ, Houten SM. Increased cardiac fatty acid oxidation in a mouse model with decreased malonyl-CoA sensitivity of CPT1B [Internet]. Cardiovascular Research. 2018;114:1324–1334. Available from: http://dx.doi.org/10.1093/cvr/cvy089
34. Shi J, Qu Q, Liu H, Zhang Y, Cui W, Chen P, Lv H. Case Report: PNPLA2 Gene Complex Heterozygous Mutation Leading to Neutral Lipid Storage Disease With Myopathy. *Front Integr Neurosci* [Internet]. 2021 [cited 2021 Jul 27];14. Available from: https://pubmed.ncbi.nlm.nih.gov/33551761/
35. Rech M, J J F, Glatz JFC, van Bilsen M, Schroen B, Nabben M. Assessing fatty acid oxidation flux in rodent cardiomyocyte models [Internet]. Scientific Reports. 2018;8. Available from: http://dx.doi.org/10.1038/s41598-018-19478-9
36. Martínez MS, García A, Luzardo E, Chávez-Castillo M, Olivar LC, Salazar J, Velasco M, Quintero JJR, Bermúdez V. Correction: Energetic metabolism in cardiomyocytes: molecular basis of heart ischemia and arrhythmogenesis [Internet]. Vessel Plus. 2018;2:32. Available from: http://dx.doi.org/10.20517/2574-1209.2018.68
37. Haffar T, Bérubé-Simard F, Bousette N. Impaired fatty acid oxidation as a cause for lipotoxicity in cardiomyocytes. Biochem Biophys Res Commun. 2015;468:73–78.
38. Hickson-Bick DLM, Buja ML, McMillin JB. Palmitate-mediated Alterations in the Fatty Acid Metabolism of Rat Neonatal Cardiac Myocytes [Internet]. Journal of Molecular and Cellular Cardiology. 2000;32:511–519. Available from: http://dx.doi.org/10.1006/jmcc.1999.1098
39. Hong F, Xu P, Zhai Y. The Opportunities and Challenges of Peroxisome Proliferator-Activated Receptors Ligands in Clinical Drug Discovery and Development [Internet]. International Journal of Molecular Sciences. 2018;19:2189. Available from: http://dx.doi.org/10.3390/ijms19082189
40. Home P. Safety of PPAR agonists. Diabetes Care. 2011;34 Suppl 2:S215–9.
41. Burke MA, Chang S, Wakimoto H, Gorham JM, Conner DA, Christodoulou DC, Parfenov MG, DePalma SR, Eminaga S, Konno T, Seidman JG, Seidman CE. Molecular profiling of dilated cardiomyopathy that progresses to heart failure. *JCI Insight* [Internet]. 2016;1. Available from: http://dx.doi.org/10.1172/jci.insight.86898
42. Pascual F, Coleman RA. Fuel availability and fate in cardiac metabolism: A tale of two substrates. Biochim Biophys Acta. 2016;1861:1425–1433.
43. Fillmore N, Lopaschuk GD. Targeting mitochondrial oxidative metabolism as an approach to treat heart failure [Internet]. Biochimica et Biophysica Acta (BBA) - Molecular Cell Research. 2013;1833:857–865. Available from: http://dx.doi.org/10.1016/j.bbamcr.2012.08.014
44. Davargaon RS, Sambe AD, V SMV. Toxic effect of high glucose on cardiomyocytes, H9c2 cells: Induction of oxidative stress and ameliorative effect of trolox [Internet]. Journal of Biochemical and Molecular Toxicology. 2019;33:e22272. Available from: http://dx.doi.org/10.1002/jbt.22272
45. Taegtmeyer H, Sen S, Vela D. Return to the fetal gene program [Internet]. Annals of the New York Academy of Sciences. 2010;1188:191–198. Available from: http://dx.doi.org/10.1111/j.1749-

6632.2009.05100.x

46. Taegtmeyer H, Golfman L, Sharma S, Razeghi P, Arsdall M. Linking Gene Expression to Function: Metabolic Flexibility in the Normal and Diseased Heart [Internet]. Annals of the New York Academy of Sciences. 2004;1015:202–213. Available from: http://dx.doi.org/10.1196/annals.1302.017
47. Bround MJ, Wambolt R, Luciani DS, Kulpa JE, Rodrigues B, Brownsey RW, Allard MF, Johnson JD. Cardiomyocyte ATP production, metabolic flexibility, and survival require calcium flux through cardiac ryanodine receptors in vivo. J Biol Chem. 2013;288:18975–18986.
48. Pinto AR, Ilinykh A, Ivey MJ, Kuwabara JT, D'Antoni ML, Debuque R, Chandran A, Wang L, Arora K, Rosenthal N, Tallquist MD. Revisiting Cardiac Cellular Composition. Circ Res. 2016;118:400.
49. Pingzhu Zhou WTP. Recounting cardiac cellular composition. Circ Res. 2016;118:368.

Figures

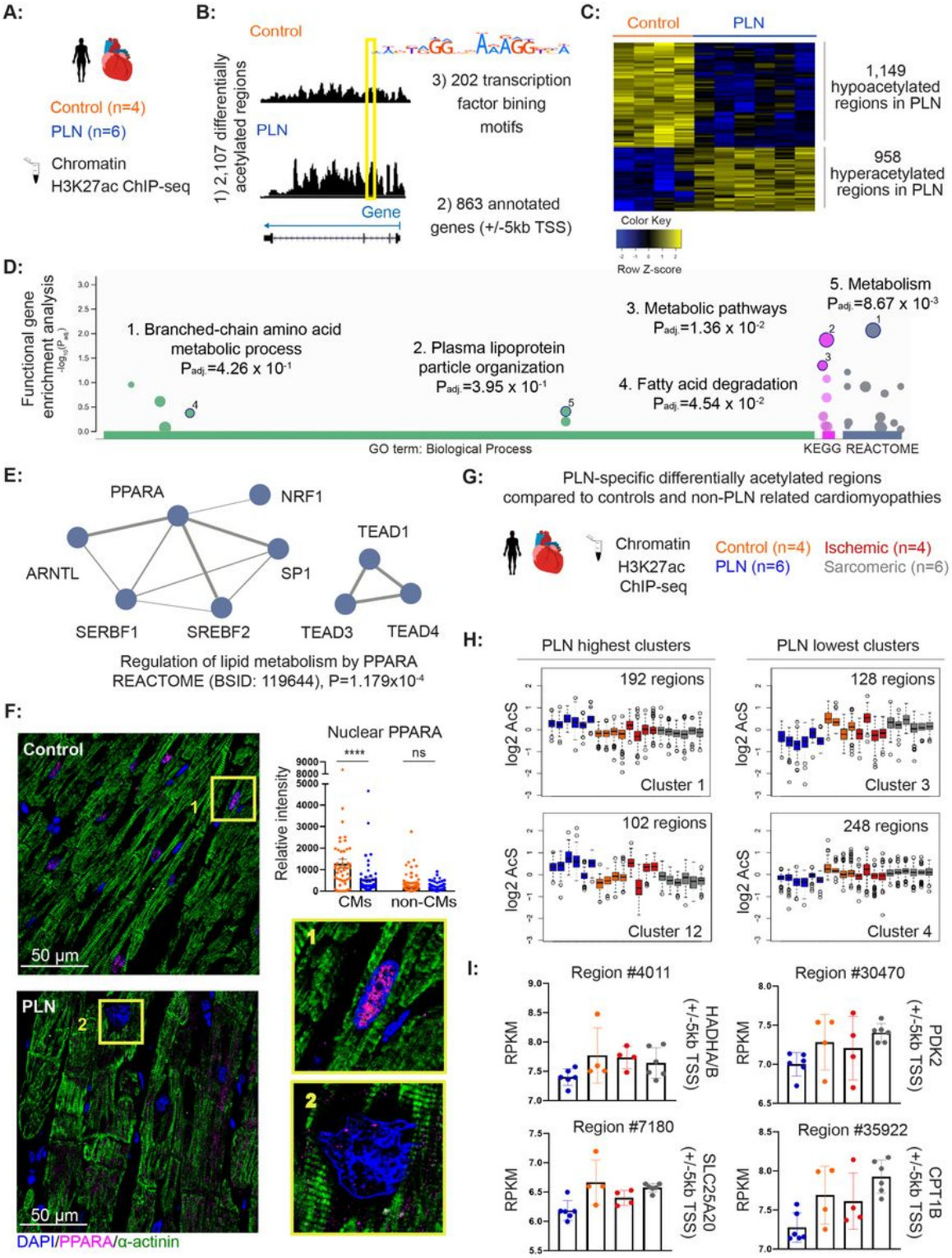

Figure 1

Identification of differentially acetylated DNA regulation regions in PLN-R14del cardiomyopathy compared to the controls and other cardiomyopathies. A) An overview illustrating the study design of comparing histone acetylation between PLN-R14del cardiomyopathy and the healthy controls using H3K27ac ChIP-seq. **B)** A workflow indicating the production of three main datasets obtained from identified histone acetylated regions: dataset 1) 2,107 differentially acetylated regions between PLN-

R14del and controls; dataset 2) 863 genes annotated to differentially acetylated regions in the +/-5kb window from the gene's transcription start site; dataset 3) 202 transcription factor binding motifs (TFBMs) enriched within the sequences of differentially acetylated regions. **C)**Heatmap showing top 100 differentially acetylated regions in cardiac tissue from PLN-R14del versus control hearts (dataset 1). **D)** Functional gene enrichment analysis using annotated genes in the vicinity of hypoacetylated regions pointed towards altered metabolism-related biological functions (dataset 2). **E)**PPARA and its interacting TFs involved in lipid metabolism obtained from TFBMs enriched in differentially acetylated regions (dataset 3). **F)** Immunofluorescence staining and quantification of nuclear PPARA signals (magenta) in PLN-R14del and control hearts. The nucleus was stained in blue and α-actinin in green. Confocal images were taken at 63x magnification. CMs: identified cardiomyocytes in the tissues; non-CMs: non-cardiomyocytes in the tissues. **G)** An overview showing additional biopsies from patients with ischemic cardiomyopathy and sarcomeric non-ischemic cardiomyopathy (non-PLN-related cardiomyopathies), besides PLN-R14del and control hearts as indicated in A). **H)** K-mean clustering analysis showing four PLN-R14del-specific clusters based on acetylation signals (AcS). **I)** Examples of genes involved in mitochondrial metabolism annotated to regions from PLN-R14del-lowest clusters (cluster 3 and 4) shown in H).

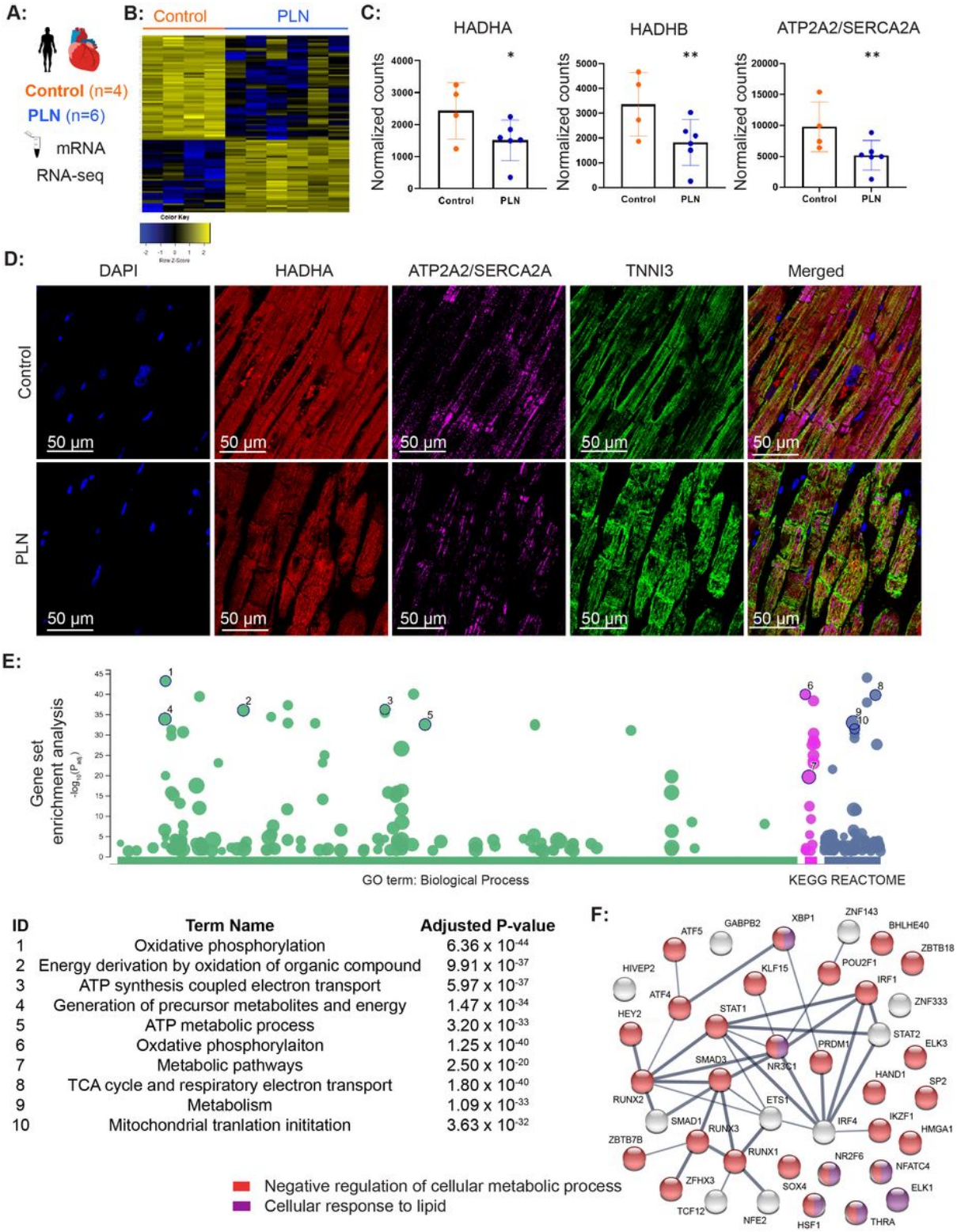

ID	Term Name	Adjusted P-value
1	Oxidative phosphorylation	6.36×10^{-44}
2	Energy derivation by oxidation of organic compound	9.91×10^{-37}
3	ATP synthesis coupled electron transport	5.97×10^{-37}
4	Generation of precursor metabolites and energy	1.47×10^{-34}
5	ATP metabolic process	3.20×10^{-33}
6	Oxdative phosphorylaiton	1.25×10^{-40}
7	Metabolic pathways	2.50×10^{-20}
8	TCA cycle and respiratory electron transport	1.80×10^{-40}
9	Metabolism	1.09×10^{-33}
10	Mitochondrial tranlation inititation	3.63×10^{-32}

Figure 2

Identification of differentially expressed genes between PLN-R14del and control hearts using RNA-seq. A) An overview illustrating the study design of comparing transcriptome between PLN-R14del and control hearts using RNA-seq after poly(A) selection. **B)** Heatmap showing top 100 differentially expressed genes in cardiac tissue from PLN-R14del versus control hearts. **C)** Examples of 3 differentially expressed genes between PLN-R14del and control hearts. **D)** PLN-R14del heart showed lower ATP2A2/SERCA2A signal

(purple) and HADHA signal (red) compared to the control heart using immunofluorescence staining, confirming its levels in the RNA-seq data. Nuclei were stained by DAPI (blue) and sarcomeres were stained by TNNI3 (green). Confocal images were taken at 63x magnification. **E)** Enrichment analysis using downregulated genes indicated the top enriched biological processes and pathways were related to metabolism. **F)** Protein-protein-interaction network using 39 TFs from the integrative analysis pointed toward (negatively) affected metabolism. Protein-coding genes involved in “Negative regulation of cellular metabolic process” are shown in red, protein-coding genes involved in “Cellular response to lipid” are shown in purple, and protein-coding genes that are not involved in these two processes are shown in light grey.

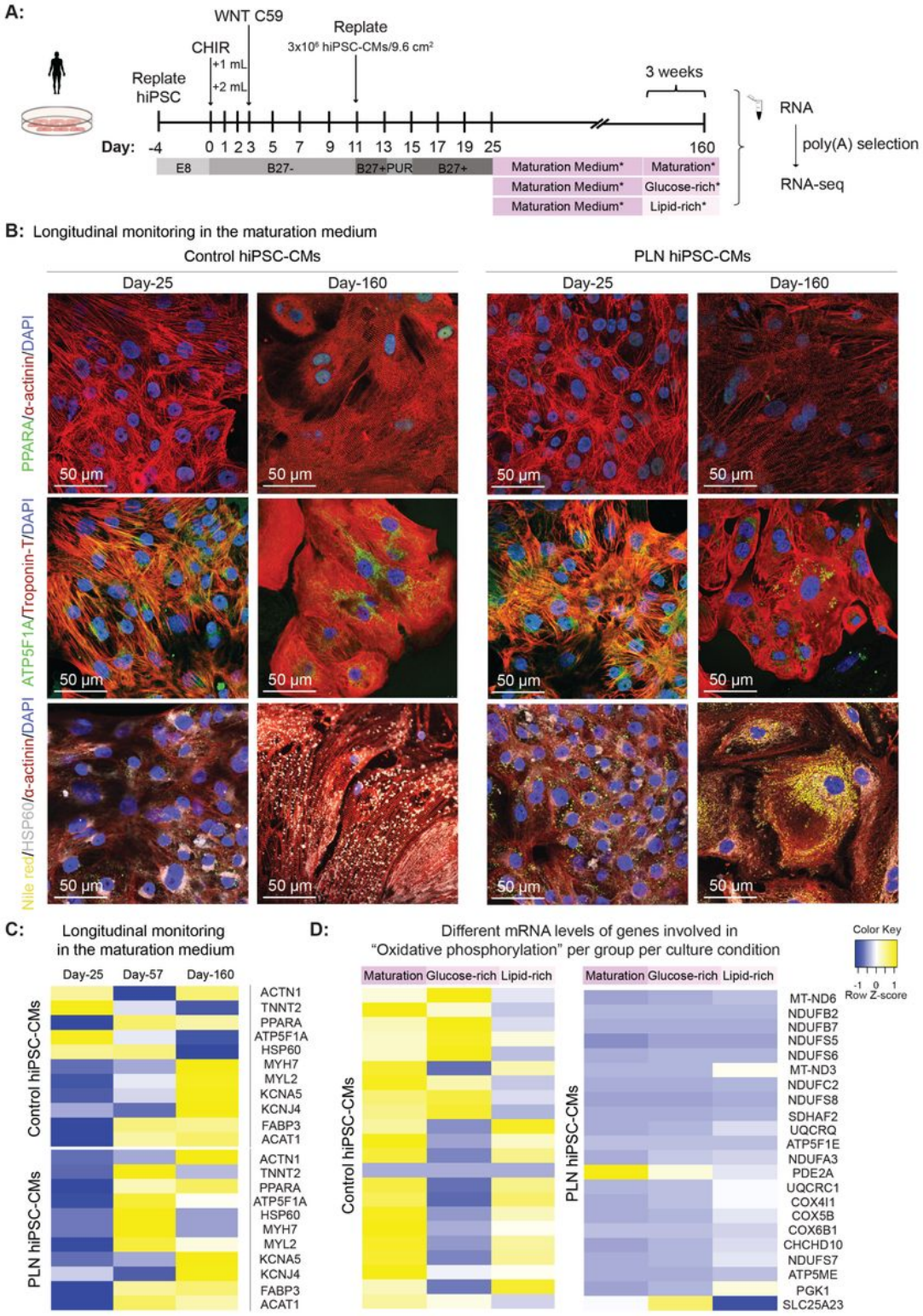

Figure 3

Characterization of long-term cultured human induced pluripotent stem cell-derived cardiomyocytes (hiPSC-CMs) and identification of differentially expressed genes between PLN-R14del and control hiPSC-CMs. A) An overview illustrating the study design of comparing transcriptome between long-term cultured PLN-R14del and control hiPSC-CMs in three different media. **B)** Metabolic marker (PPARA), sarcomeric markers (alpha-actinin and troponin-T), mitochondrial markers (ATP5A and HSP60), and lipid droplets

(Nile red) were examined in short-term (20 days) and long-term (160 days) cultured PLN-R14del and control hiPSC-CMs using immunofluorescence staining. Nuclei were stained by DAPI (blue). Confocal images were taken at 63x magnification. **C)** Heatmap showing the mRNA expression levels of selected markers in sarcomeres, ion channels, and metabolism in both PLN-R14del and control hiPSC-CMs were shown from the proliferation stage to the maturation stage. **D)** Heatmap showing the mRNA expression levels of genes involved in oxidative phosphorylation (GO: 0006119) in control and PLN-R14del hiPSC-CMs cultured in three different media.

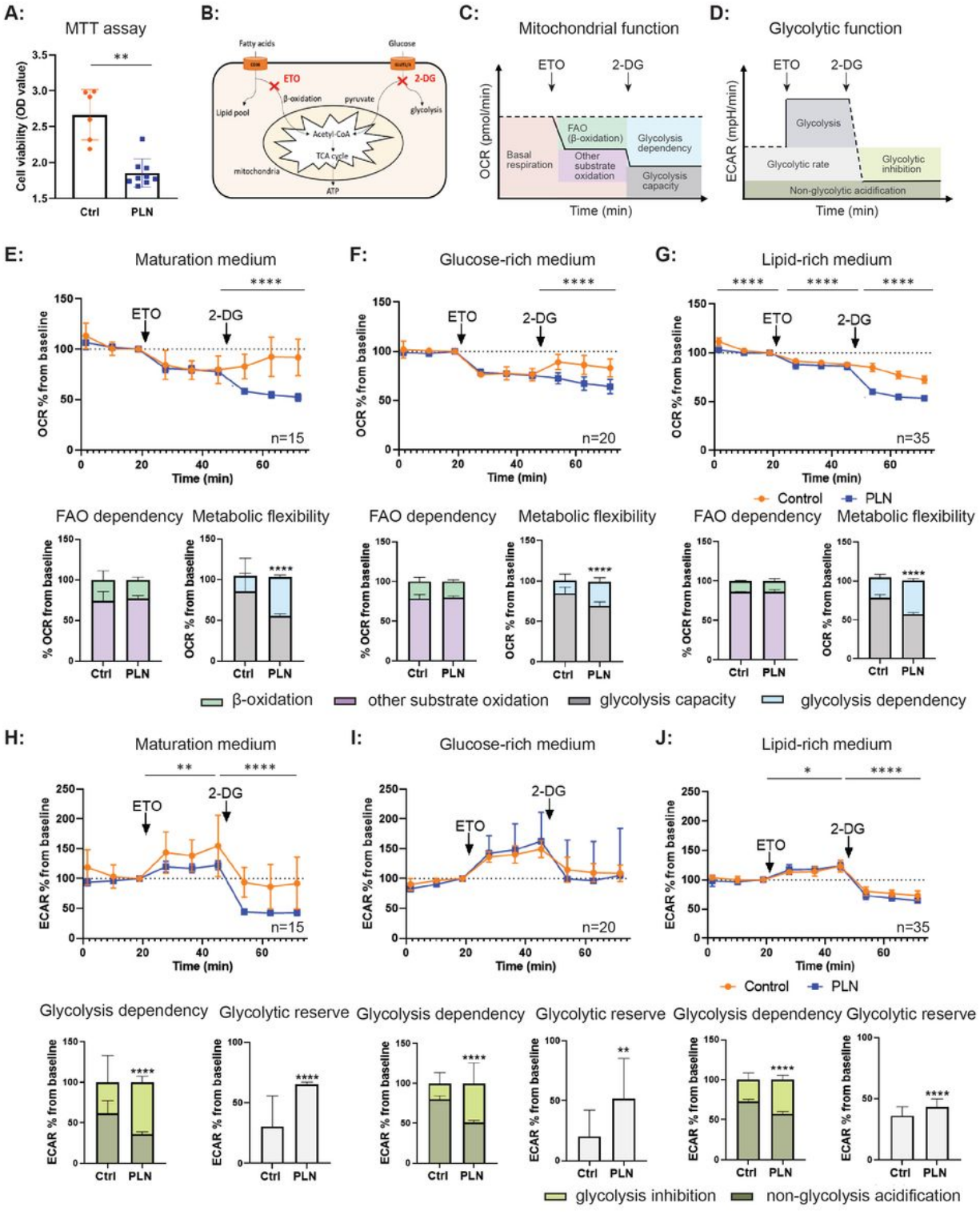

Figure 4

Examination of metabolic activity between PLN-R14del and control hiPSC-CMs. A) Tetrazolium assay showed a significantly lower general metabolic activity in PLN-R14del hiPSC-CMs when compared to the controls. **B)** A simple diagram illustrating utilization pathways of fatty acids and glucose in cardiomyocytes and two commonly used compounds, etomoxir (ETO) and 2-deoxyglucose (2-DG), to study the capacity of these pathways by blocking their utilization, respectively. **C)** An overview illustrating Seahorse XF24 Extracellular Flux assay, which measures the oxygen consumption rate (OCR) to study the activity of the fatty acid oxidation (FAO) in PLN and wild-type hiPSC-CMs by manipulating the FAO and glucose metabolism using etomoxir (ETO) and 2-deoxyglucose (2-DG). **D)** An overview illustrating Seahorse XF24 Extracellular Flux assay, which measures extracellular acidification rate (ECAR) to study the activity of the glycolytic pathway in PLN-R14del and wild-type hiPSC-CMs by manipulating the FAO and glucose metabolism using ETO and 2-DG. **E-G)** OCR of hiPSC-CMs cultured in the maturation medium, the glucose-rich medium, and the lipid-rich medium, respectively (grey arrow indicates a switch in energy substrates). Quantification of OCR values at the basal level, after ETO injection, and after 2-DG injection, were normalised to nuclei count. The degree of FAO dependency is determined by the reduction of mitochondrial function after ETO injection, and the degree of metabolic flexibility is determined by the OCR after 2-DG injection. **H-J)** ECAR of hiPSC-CMs cultured in the maturation medium, the glucose-rich medium, and the lipid-rich medium, respectively (grey arrow indicates a switch in energy substrates). Quantification of ECAR values at the baseline level, after ETO injection, and after 2-DG injection, were normalised to nuclei count. The degree of glycolysis dependency is determined by the total glycolysis minus the non-glycolytic acidification (after 2-DG injection). The glycolytic reserve ability is determined by ECAR after ETO injection minus ECAR after 2-DG injection. Data are expressed as mean ±SD, biological replicates are 3 individual differentiations with each N= 5-12 wells. One-way ANOVA with Tukey's post-hoc comparison or Student's t-tests were used, *P<0.05, **P<0.01, ***P<0.001, ****P<0.0001.

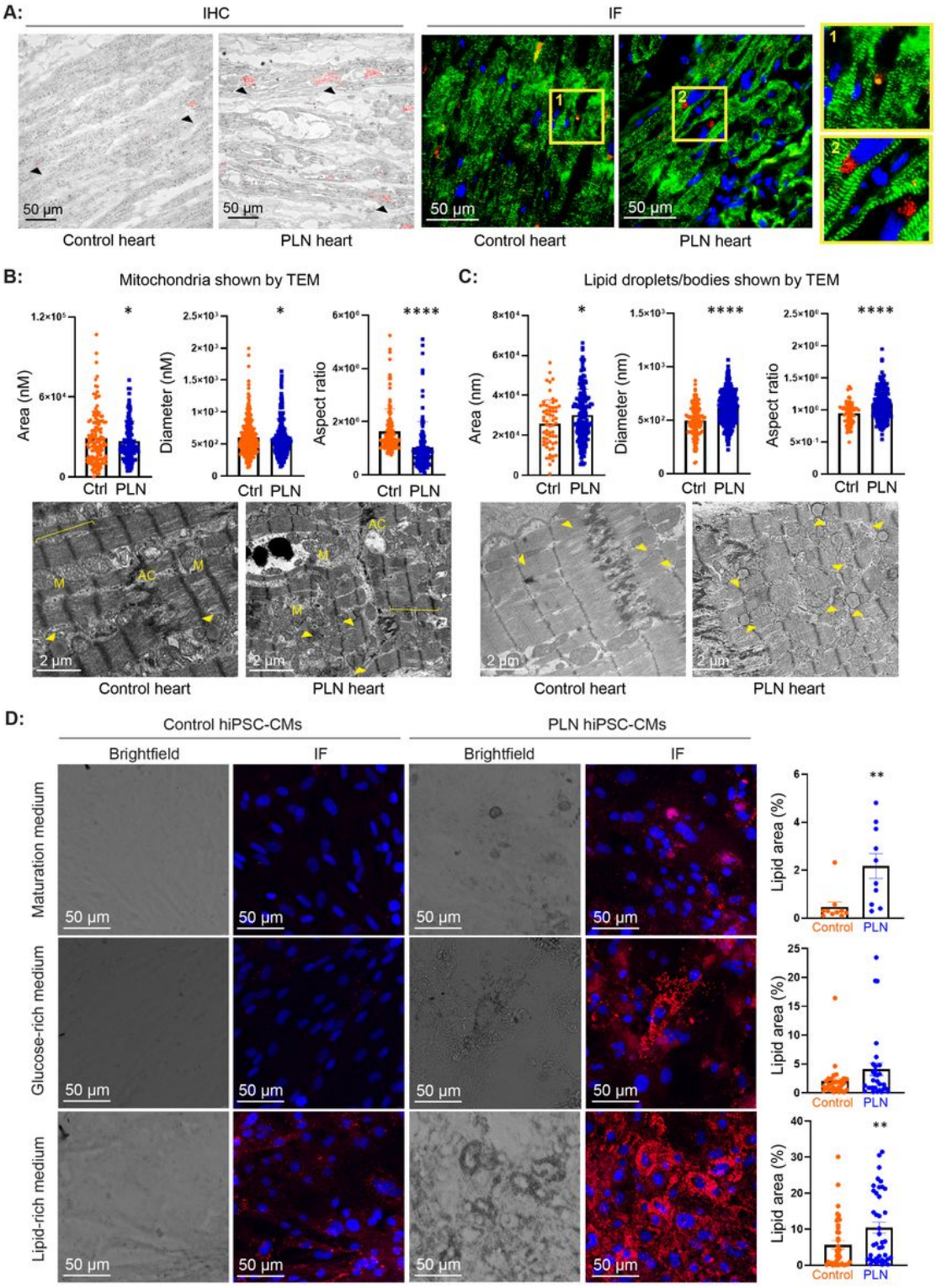

Figure 5

Lipid accumulation and impaired mitochondria in PLN-R14del cardiac tissues and hiPSC-CMs. A) Left: Examples of Nile red staining (red, indicated by black arrows) in control and PLN-R14del paraffin-embedded cardiac tissues using immunohistochemical staining (IHC). Images were taken at 40x magnification. Right: Examples of Nile red staining (red) in control and PLN-R14del snap-frozen cardiac tissues using immunofluorescence staining (IF). Confocal images were taken at 63x magnification.

Nuclei were stained by DAPI (blue) and sarcomeres were stained by TNNI3 (green). **B)** Bar graphs showing impaired detected mitochondria in PLN-R14del versus control hearts using transmission electron microscopy (TEM). Each dot represents an individual mitochondrial from control and PLN hearts. Representative TEM image of the control heart (bottom left) showing regular myofilaments arranged in sarcomeres (brackets), variable-sized mitochondria (M) arranged in rows in between myofibrils, lipid droplets (yellow arrows) and profiles of the intercalated disc with a large mixed-type junction (*area composita*, AC) in between cardiomyocytes. Whereas, representative TEM image of the PLN-R14del heart (bottom right) shows irregular myofilaments arranged in sarcomeres (brackets), variable-sized mitochondria (M) located around the myofibrils, lipid droplets (yellow arrows) and profiles of the intercalated disc with a large mixed-type junction (AC) in between cardiomyocytes. Multiple shape descriptors were determined for manually traced lipid droplets and mitochondria. **C)** Bar graphs showing higher coverage by lipid droplets and bigger lipid droplets in PLN-R14del versus control hearts using TEM. Representative TEM images (below) showing manually traced lipid droplets (indicated by yellow arrows) in the control and PLN-R14del hearts. Each dot represents an individual lipid droplet from control and PLN hearts. TEM images were collected from 3 healthy controls (67 traced lipid droplets and 128 traced mitochondria) and 1-2 PLN-R14del hearts (177 traced lipid droplets and 129 traced mitochondria). Data are expressed as mean ±SD. Unpaired T-test was used, *P<0.05, ****P<0.0001. Scale bar: 2 μM. **D)** Examples of Nile red staining to demonstrate the lipid accumulation in long-term cultured (160 days) PLN-R14del and control hiPSC-CMs in three different media. Bar graph showing a higher lipid accumulation (red) in PLN-R14del versus control hiPSC-CMs in three different media.

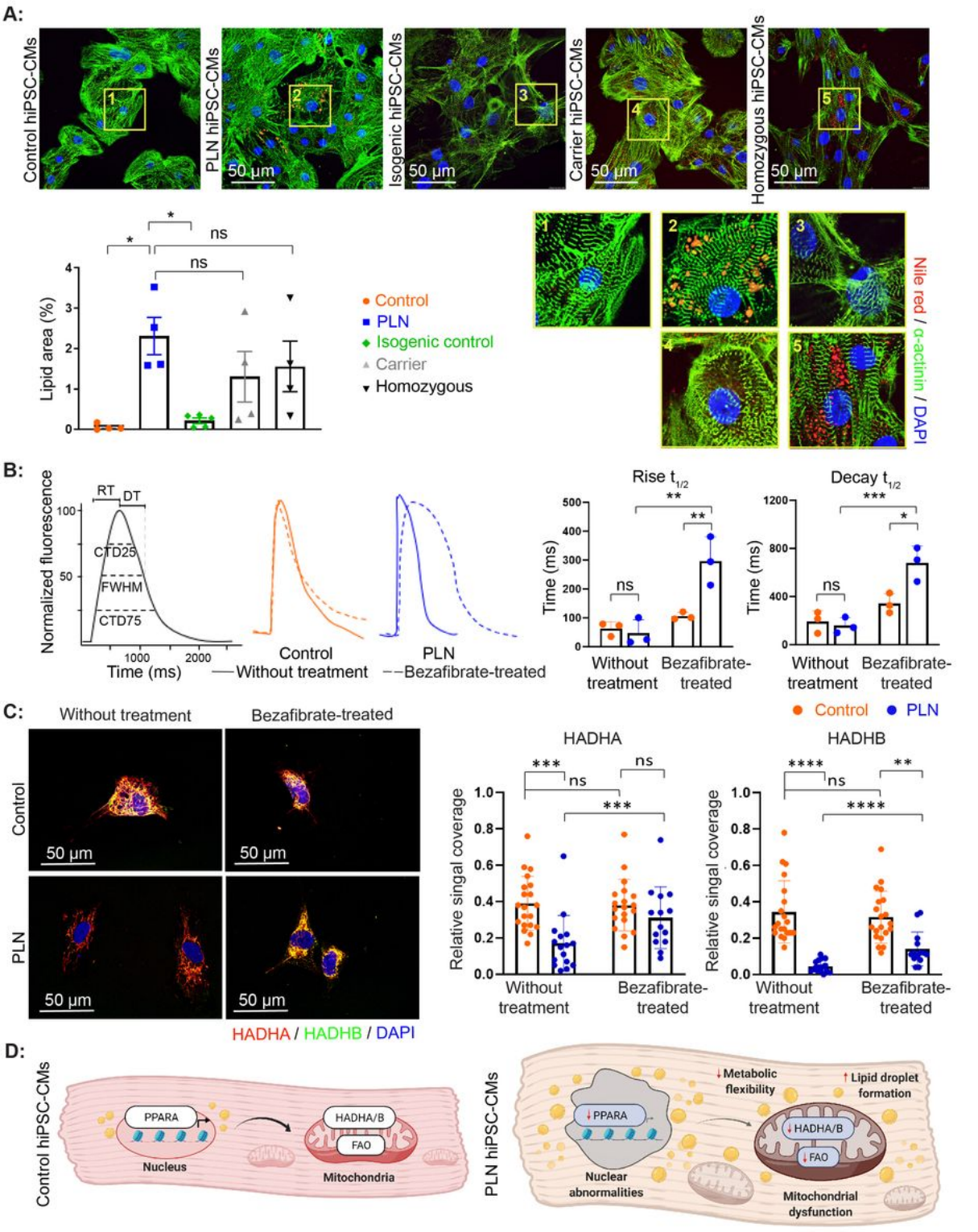

Figure 6

Genetic engineering and agonist therapy as novel treatment strategies targeting dysregulated lipid metabolism in PLN-R14del cardiomyopathy. A) Immunofluorescence images of Nile red staining showing the lipid accumulation in all hiPSC-CMs groups. Nuclei were stained by DAPI (blue). Bar graph showing a significantly higher intracellular lipid formation in PLN-R14del hiPSC-CMs when compared to the healthy controls as well as the isogenic controls in which PLN-R14del was corrected (n ≥ 4 per group), whereas

the lipid accumulation in hiPSC-CMs from PLN-R14del patient, an asymptomatic PLN-R14del carrier, and a homozygous PLN-R14del group reamined comparable. Data were normalised to nuclei and shown as mean ±SEM. One-way ANOVA was used, **P<0.01, ***P<0.001. **B)** Ca^{2+} transient parameters for examining the Ca^{2+} handling property in hiPSC-CMs, including rise time (RT), decay time (DT), calcium full width half maximum (FWHM), duration at 25% decline from maximum amplitude (CTD25), and duration at 75% decline from maximum amplitude (CTD75). Representative calcium transient in control and PLN-R14del hiPSC-CMs with and without bezafibrate treatment (solid and dashed line, respectively). Each trace is an average DF/F 0 versus time plot (33 Hz) in each well and three wells per condition per group were included in this analysis. **C)** Immunofluorescence staining of HADHA (red) and HADHB (green) in control and PLN-R14del hiPSC-CMs with and without bezafibrate treatment. Nuclei were stained by DAPI (blue). All images were taken at 63x magnification. Bar graphs showing significantly elevated HADHA and HADHB levels after bezafibrate treatment in PLN-R14del, but not in the control hiPSC-CMs. Data was normalised to the number of nuclei. Each dot represents the normalized data per obtained images and shown as mean ±SD. Two-way ANOVA was used in the bezafibrate treatment experiment, ns= not significant, **P<0.01, ***P<0.001, ****P<0.0001. **D)** Schematic overview of PPARA-mediated FAO dysregulation and impaired lipid metabolism in PLN-R14del versus control cardiomyocytes.

Supplementary Files

This is a list of supplementary files associated with this preprint. Click to download.

- FigureS1.png
- FigureS2.png
- FigureS3.png
- FigureS4.png
- FigureS5.png
- FigureS6.png
- FigureS7.png
- FigureS8.png
- FigureS9.png
- FigureS10.jpg
- SUPPLEMENTARYMETHODS.docx
- TableS1.xlsx
- TableS2.xlsx
- TableS3.xlsx
- TableS4.xlsx

- TableS5.xlsx
- TableS6.xlsx
- TableS7.xlsx
- TableS8.xlsx
- Supplmentaryvideo1CtrlDay12.avi
- Supplmentaryvideo2CtrlDay90.avi
- Supplmentaryvideo3PLNDay12.avi
- Supplmentaryvideo4PLNDay90.avi